This is an extended version of the paper presented in SEE7 conference, peer-reviewed again and approved by the JSEE editorial board.

Seismic Response of 2D Triangular-Shaped Alluvial Valleys to Vertically Propagating Incident SV Waves

Peyman Aminpour[1*], Jafar Najafizadeh[2], Mohsen Kamalian[3], and Mohammad Kazem Jafari[3]

1. M.Sc. Graduate of Geotechnical Engineering Research Center, International Institute of Earthquake Engineering and Seismology (IIEES), Tehran, Iran,
* Corresponding Author; email: p.aminpour@iiees.ac.ir
2. Ph.D. Graduate of Geotechnical Engineering Research Center, International Institute of Earthquake Engineering and Seismology (IIEES), Tehran, Iran
3. Professor, Geotechnical Engineering Research Center, International Institute of Earthquake Engineering and Seismology (IIEES), Tehran, Iran

Received: 11/01/2015
Accepted: 13/12/2015

ABSTRACT

This paper presents the results of a numerical parametric study on the seismic behavior of 2D triangular-shaped valleys subjected to vertically propagating incident SV waves. The medium is assumed to have a linear elastic constitutive behavior. All calculations are executed in time-domain utilizing the spectral finite element method. Clear perspectives of the amplification patterns of the valley are presented by investigation of the frequency-domain responses. It is shown that the amplification pattern of the valley and its frequency characteristics depend strongly on its shape ratio. The maximum amplification ratio along the ground surface occurs at the centre of the valley. A simple formula has been proposed for making initial estimation of the natural period of the valley in site effect microzonation studies. The natural frequency of the alluvial valley decreases as the shape ratio of the valley decreases; moreover, the value of the natural frequency of the triangular alluvial valley is bigger than the natural frequency of the corresponding rectangular alluvial valley.

Keywords:
Triangular alluvial valleys; Amplification; Site effects; Topography effect; Spectral finite element; Wave propagation

1. Introduction

It is well-known to the discipline of geotechnical earthquake engineering that site effects and local conditions can exert large amplifications and important spatial variations of ground shaking. There is a close relation between earthquake damage and topographic and geological irregularities. This fact has been substantiated by the reported variability of ground shaking or the non-uniform distribution of damage during numerous strong earthquakes in recent years alleging that one-dimensional (1-D) analysis cannot sufficiently explain the seismic behavior of subsurface irregularities.

Various analytical or numerical simulations have suggested that the existence of subsurface irregularities, like alluvial valleys or sedimentary basins can exert a profound influence on the surface ground motion, notably by altering the frequency content, prolonging the duration of shaking or by aggravating the amplitude of motion [1-14]. The main phenomena that constitute the "valley amplification" effects on site response have been summarized for the geotechnical community by Aki [2] and Finn [15]; some newer major seismic events have dramatically reinforced their main conclusions.

The damage distribution observed during the 1988 Armenia earthquake is the archetype of "valley amplification" effects on site response. Yegian et al. [16], trying to correlate the observed damage with the ground shaking in the city of Kirovakan, located about 10 to 15 km from the surface outbreak of the fault, pointed out that 1D analyses substantially underestimated the ground surface motion in a region of Kirovakan in which the soil profile constitutes a triangular alluvial valley whose width is only about five times its depth. A satisfactory explanation for the observed damage was adequately presented by Bielak et al. [13] who conducted two-dimensional (2-D) ground response analyses for the same valley. As another illustration of the "valley amplification", numerical studies have also shown that the aggravation of damage reported in the Marina District, San Francisco, during the 1989 Loma Prieta earthquake, could be generally attributed to the 2D site conditions [17-19]. Graves [20], simulating the seismic response of the San Fernando basin in the 1994 Northridge earthquake, showed that the subsurface irregularities may have caused a large amplification, especially in the long period ground motions. Finally, during the 1995 Hyogoken-Nambu earthquake, most of the damage in the city of Kobe occurred within the so-called "disaster belt", a narrow zone 1 km wide, nearly 20 km long, located between about 1 to 1.5 kilometers from the Rokko mountain rock outcrop. Numerical analyses by various researchers [12, 21-25] have underlined the need for doing 2D simulations in order to capture correctly the valley amplification.

Several methods have been utilized to analyze the seismic response of basins and alluvial valleys. Analytical techniques can be applied only for simple geometries and homogeneous deposits that allow the separation of variables of the governing equations (e.g., [26-29]. For simulations of realistic basins and valleys with irregular shapes and heterogeneous deposits and alluvial materials, numerical procedures become essential. The most widely used ones include the finite-difference method (e.g., [30], [31] in 2D, and [32] in 3D), the finite-element method (e.g., [9, 33-36], the boundary element method (e.g., [28, 37-43], and hybrid type methods, which combine the effective characteristics of two or more methods, such as the hybrid BE/FE method (e.g., [13, 44].

The present study analyzes numerically the effects of the triangular alluvial valley on its ground surface seismic motion utilizing a Spectral-Finite-Element code developed by Najafizadeh and Kamalian [45]. The "confinement" of seismic waves in the valley and the generation of surface waves at the edges of the valley are phenomena expected to have the following "valley amplification" effects: 1- The aggravation of the ground shaking may be amplified more than 1D wave-theory predicts. 2- The spatial variability of the ground surface motion may be substantial.

The goal of this paper is to capture numerically "valley amplification" effects on the surface ground motion of triangular alluvial valleys, and to find out the answers of the following questions: What is the maximum amplification potential of the valley? Where does it occur along the valley? How does the amplification pattern vary along the valley? Does increasing the shape ratio (ratio of height to half-width) of the valley necessarily mean intensifying the amplification potential at any point along it? Is it possible to extract a simple formula in order to get an initial estimation of the natural period of the alluvial valley for microzonation studies?

2. Analyze the Walley

2.1. Characteristics of the Valleys and Basis Excitation

The valley, the seismic behavior of which is examined in current study, constitutes a wide spectrum of triangular alluvial valleys with various shape ratios. The geometry of the 2D homogenous isotropic linearly elastic alluvial valley is depicted in Figure (1) where H and ax denote the thickness of center line and the half-width of the soil layer along the ground surface, respectively. The surrounding bedrock is assumed to be rigid.

Inasmuch as altering the basis excitation would not influence the amplification pattern in a linear elastic media, the incident wave is chosen as the well-known Ricker type, Figure (2), with the following equation:

$$f(t) = A_{\max}[1-2(\pi f_p(t-t_0))^2]e^{-(\pi f_p(t-t_0))^2} \qquad (1)$$

where f_p, t_0 and $A_{\max}$ denote the predominant frequency, the time shift parameter and the

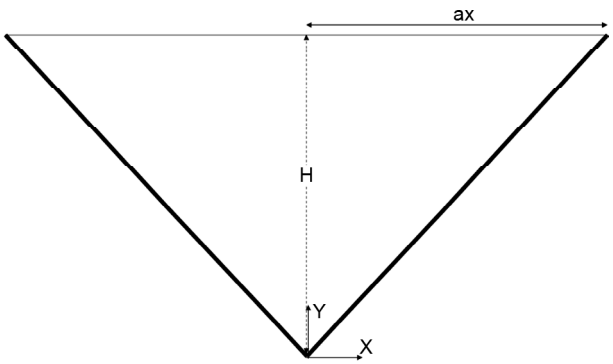

Figure 1. Geometry of the 2D homogenous triangular alluvial valley. H and ax denote the thickness of center line and the half-width of the soil layer along the ground surface, respectively.

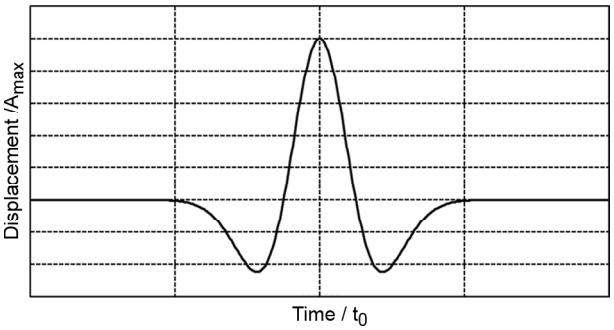

Figure 2. Displacement time history of the incident wave.

maximum amplitude of the displacement time history, respectively.

2.2. Method of Analysis

The mathematical problem under consideration is a wave propagation from a rigid bedrock into an alluvial valley with a homogeneous soil and irregular geometries. The governing equation for an isotropic, homogeneous, small-displacement body with linear elastic behavior can be written as the equilibrium equations for an elastic bounded medium $\Omega \subset R_d$ subjected to an external body-force f_i:

$$\sigma_{ij,j} + f_i = \rho \ddot{u}_i, \quad i = 1,...,d \tag{2}$$

where $\sigma_{ij}n_i$. denotes the stress tensor components; ρ, is the mass density, and $\ddot{u}_i = \partial^2 u_i / \partial t^2$ is the second derivative of displacement of the medium with respect to time. By using the weighted residual approach, the matrix form of the governing equation is obtained.

$$M \cdot \ddot{U} + K \cdot U = F \tag{3}$$

where:

$$K = \sum_m K^m$$
$$M = \sum_m M^m \tag{4}$$
$$F = \sum_m \left(f_{\Gamma_m - u} + f_{\Omega_m - u} \right)$$

U = vector of time-dependent nodal displacements; an overdot denotes differentiation with respect to time; M, C, and K = global mass, damping, and stiffness matrices; and F = vector of equivalent nodal forces. If material damping is assumed in the medium, Eq. (3) can be rewritten as follows:

$$M \cdot \ddot{U} + C \dot{U} + K \cdot U = F \tag{5}$$

In this research, the well-known Rayleigh damping mechanism was used which can be expressed proportional to the mass and stiffness matrixes as follows:

$$C = a_0 M + a_1 K \tag{6}$$

Basically, it was strived to analyze the "valley amplification" effects on the ground surface motion of the valley when soil behaves linearly. It has been observed in many cases that soft soil layers could be assumed to have a linear behavior because of two reasons [46]. The first reason is that approximately even the strongest earthquakes were characterized by low acceleration levels, while the second one is that the soft soil layers were generally characterized by large PI, behaving almost linearly even at large strain levels. In this study linear 2-D ground response analyses were conducted, utilizing one numerical model, based on the Spectral-Finite-Element method (SFEM). In this model, an incident SV wave excitation was induced.

The linear SFEM modeling was performed by NASEM, an advanced code of the two-dimensional spectral finite element analyses, developed by Najafizadeh et al. [45]. The advantage of this method is that, by using a special group of interpolation functions, Eq. (7), the SFEM is able to pass a wider range of wavelengths in the elements with more careful and less computational efforts than that of the conventional FEM, and by using fewer meshing points an equal degree of accuracy is gained. These specific interpolation functions are achieved by implementing Legendre-Gauss-Lobatto (LGL) points in Lagrange polynomials of degree.

$$h_n^{n_l}(\xi) = \frac{(\xi-\xi_1)(\xi-\xi_2)...(\xi-\xi_{n-1})(\xi-\xi_{n+1})...(\xi-\xi_{n_l+1})}{(\xi_n-\xi_1)(\xi_n-\xi_2)...(\xi_n-\xi_{n-1})(\xi_n-\xi_{n+1})...(\xi_n-\xi_{n_l+1})}; \quad -1 \le \xi \le 1, \quad n = 1,.....,n_l+1 \tag{7}$$

Place of the control points is determined through solving the following equations:

$$(1-\xi^2) * L'_{n_l}(\xi) = 0 \quad , \quad (1-\eta^2) * L'_{n_l}(\eta) = 0 \tag{8}$$

where, L'_{n_l} is first derivative of Lagrange polynomials of degree n_l.

By using these control points, the computational errors decline exponentially. This method can converge faster to the precise solution than FEM due to using fewer degrees of freedom with almost the same accuracy. A highly interesting property of the SFEM is the fact that the mass matrix [*M*] is diagonal due to using LGL quadrature for each element [47]. This allows for a very significant reduction in computational cost and complexity. In this model, the basis excitation is implemented as an incident plane SV wave obtained by exerting the same acceleration to all nodal points belonging to the boundary lines, and rigid boundaries were placed around the domain of interest.

The spectral-element mesh, Figure (3), is made up of some quadrilateral (2D) non-overlapping elements Ω_e. The size of the elements has also been tailored to the local wavelength of the propagating waves. An expansion in terms of a tensor-product of N^{th}-order orthogonal polynomials is used to approximate solution, data, geometry and physical properties on each element.

After assembly of the individual mass, damping, and stiffness matrices, and of the equivalent seismic forces, Eq. (3) has been solved numerically by the implicit, unconditionally stable Newmark's step-by-step method with $\delta = 0.5$ and $\alpha = 0.25$. Selection of time step Δt is another factor that must be taken into account when solving the system of equations. The number of the time steps influences directly the computation volume and the needed accuracy. In SFEM, in high orders, the intervals between the nodes are smaller than those of the FEM. Therefore, smaller time steps are needed for high-order spectral elements.

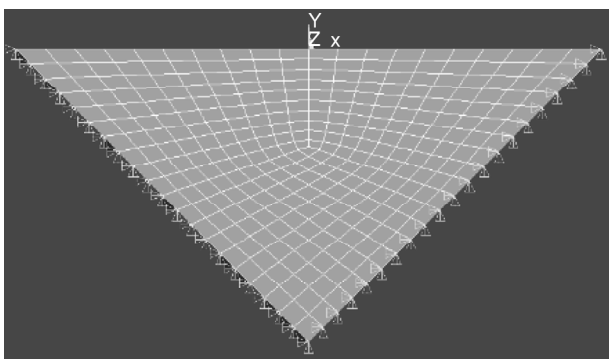

Figure 3. Spectral-element discretization of the valley. The spectral mesh is made up of some quadrilateral (2D) non-overlapping elements.

The verification of this numerical model has been performed by solving several examples including 1D site response analysis and 2D seismic behavior of rectangular alluvial valleys [45] in order to show the accuracy and efficiency of this implemented SFEM algorithm in conducting site response analysis of topographic irregularities.

To demonstrate the influence of shape ratio (ratio of height to half-width) on the valley amplification of the specific site, linear 2D ground response analyses were performed, modeling various triangular valleys with a constant depth and a wide spectrum of shape ratios (by changing the widths of valleys). While comparing seismic behavior of different alluvial valleys not only shape ratios but also the dimensions of valleys must be taken into account. It has been recognized that the ratio of the topography height to the wavelength of the incident wave is a key factor in analyzing the amplification pattern. By normalizing the frequency-domain responses of the 2D topographic structures to the same results of the corresponding 1D uniform soil layer over the bed rock, the responses of the 2D topography irregularities can become non-dimensionalized.

All calculations were executed in time-domain using the spectral finite element method. Then, to illustrate the difference between frequency characteristics of a rectangular valley and the corresponding triangular valley in different shape ratios, clear perspectives of the amplification patterns of the valleys were compared by investigation of the frequency-domain responses.

3. Parametric Study

3.1. Methodology

In order to find out the "valley amplification" effects on the surface ground motion of triangular alluvial valleys, the broad range of 2D homogenous isotropic linearly elastic triangular alluvial valleys resting on a rigid bed rock with different shape ratios (H/ax) of 0.2, 0.4, 0.6, 0.8, 1.0 and 2.0, encountered frequently in the nature, were considered. The thickness of the soil layer at the center line was selected as 50 m. The mechanical behavior of soil with values of Poisson's ratio as 0.33, damping ratio as 0.05, mass density as 2.0 t/m^3 and shear wave velocity of the medium as 300 m/s were considered. Only one value of Poisson ratio was considered, because previous works [48] showed that the Poisson ratio of the media has a less important effect on the seismic behavior of topographic features in comparison with the shape ratio. The valley was subjected to the vertically propagating incident SV wave of the Ricker type, Figure (2). The basis excitation was implemented by exerting the same acceleration to all nodal points belonging to the boundary lines, and rigid boundaries were placed around the domain of interest.

3.2. Results of Parametric Analysis

This section presents the most important results obtained by the executed parametric study, which demonstrates the general amplification pattern of 2D triangular alluvial valleys and shows how it is affected by the various parameters.

3.2.1. General Amplification Pattern

Figure (4) demonstrates frequency-domain responses of various nodes along the ground surface of 2D triangular valleys with different shape ratios subjected to a vertically propagating incident SV wave; in fact, it is a clear perspective of the amplification curves. As can be seen, the amplification pattern of the triangular alluvial valley and its frequency characteristics depend strongly on its shape ratio. In each triangular alluvial valley and irrespective of its shape ratio, the maximum amplifi-

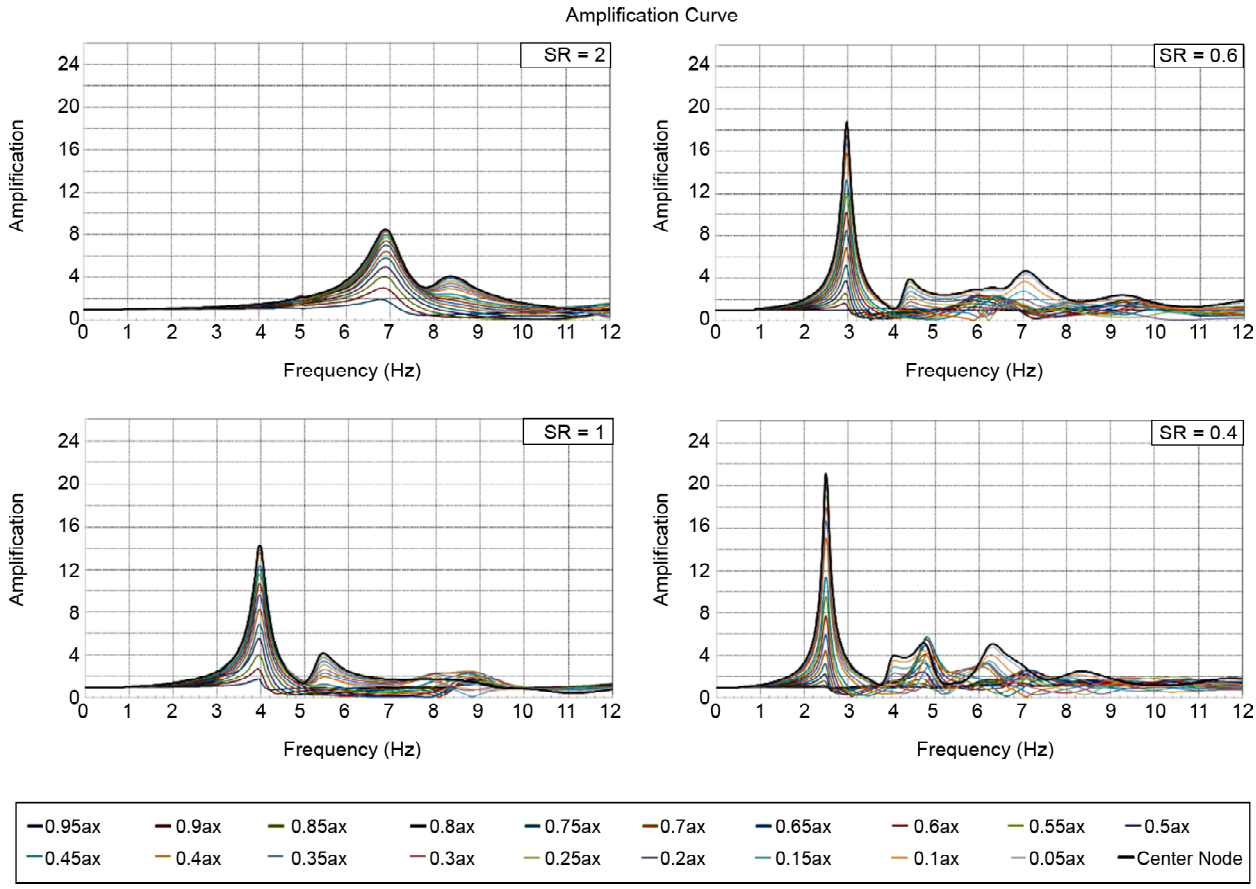

Figure 4. Variation of the amplification curves of various nodes along the ground surface of Triangular Valley (Vs = 300 m/s) via the different shape ratios.

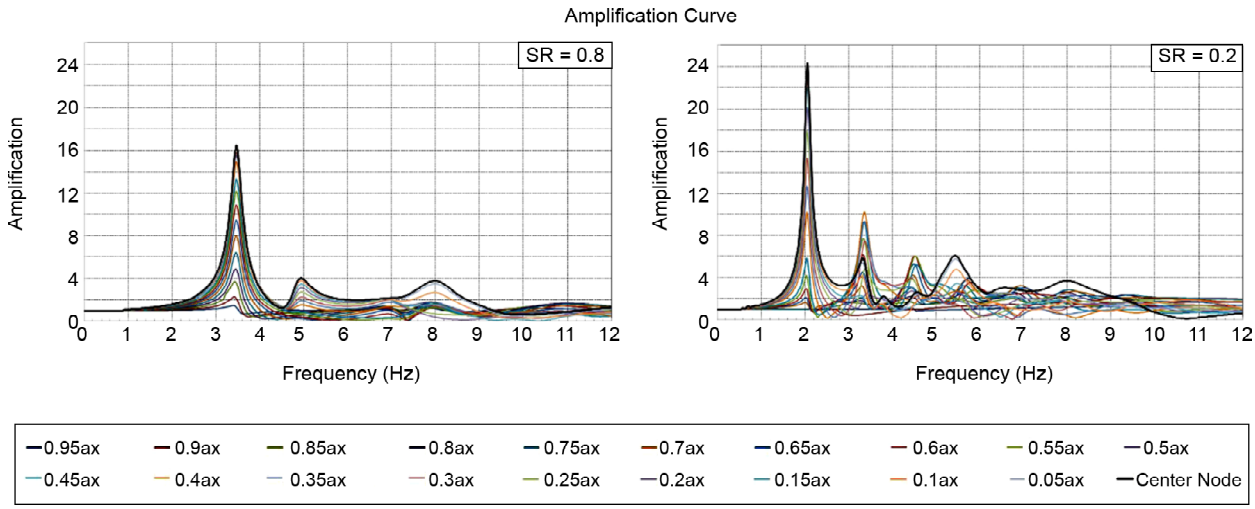

Figure 4. Continue

cation ratio at each node along the ground surface occurs at a characteristic frequency that is uniform along the ground surface. This characteristic frequency could be named as the natural frequency of the Triangular alluvial valley. The value of the natural frequency of the triangular alluvial valley decreases as the shape ratio decreases and tends towards the natural frequency of the corresponding 1D uniform soil layer over the bed rock ($W= Vs/4H$). Vice versa and as expected, the value of the natural frequency of the triangular alluvial valley increases as its shape ratio increases. It can also be seen that in each triangular alluvial valley and irrespective of its shape ratio, the maximum amplification ratio along the ground surface occurs at the center.

3.2.2. Maximum Amplification

Figure (5) illustrates the maximum amplification of various nodes along the ground surface of triangular alluvial valley via the different shape ratios normalized to the maximum amplification of a 1D uniform homogeneous soil layer resting on a rigid bed rock (amplification ratio). By normalizing the frequency-domain responses of the 2D topographic structures to the same results of the corresponding 1D uniform soil layer over the bed rock, the responses of the 2D topographic irregularities can become non-dimensionalized. As can be seen, it is substantiated that in each triangular alluvial valley and irrespective of its shape ratio, the maximum amplification ratio along the ground surface occurs at the center of the valley and by

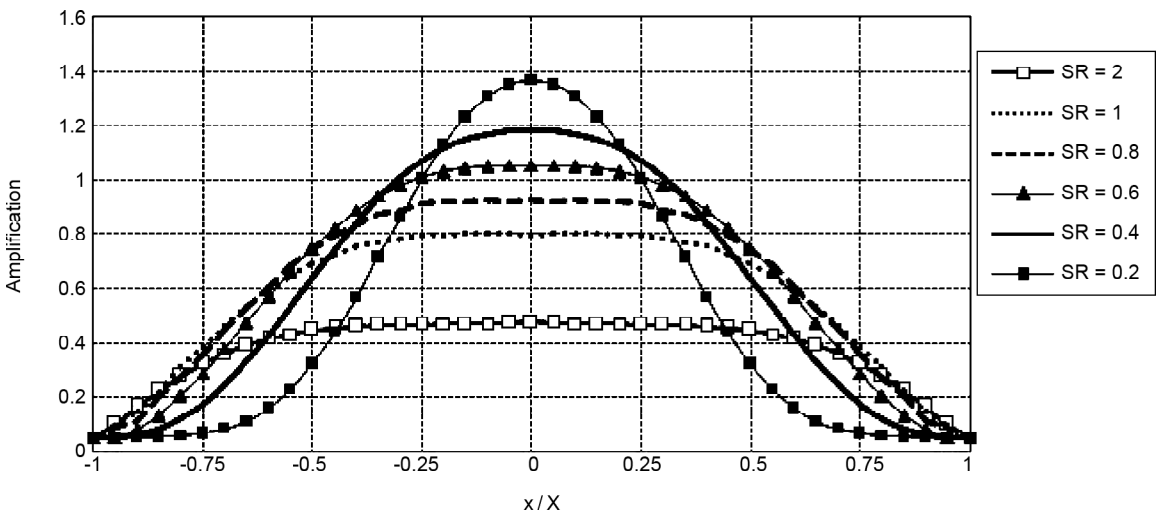

Figure 5. Comparison of the maximum amplification ratio along the ground surface of the triangular alluvial valley via the different shape ratios.

moving from each of the corners towards the center, the maximum amplification ratio of the ground surface increases. The triangular alluvial valley of the central point gets its maximum value at a shape ratio of 0.2 and decreases gradually as the shape ratio increases from 0.2 to 2.

3.2.3. Shape Ratio Effect

Figure (6) depicts the amplification curves of the center of the triangular alluvial valley with different shape ratios in comparison with the amplification curve of the corresponding 1D uniform homogeneous soil layer resting on a rigid bed rock. As can be seen, when the shape ratio decreases, the natural frequency of the triangular alluvial valley decreases, and the amplification curve of the center node (2D case) moves towards the amplification curve of the corresponding 1D case. In all triangular alluvial valleys with shape ratio of less than 0.6, the maximum amplification ratio at the center node is more than that of the corresponding 1D case; on the contrary, in the triangular alluvial valley with a shape ratio of more than 0.6 it decreases in comparison with the corresponding 1D case.

3.2.4. The Ratio of the Topography Height to the Wavelength of the Propagated Wave

Figure (7) demonstrates the effect of dimensions

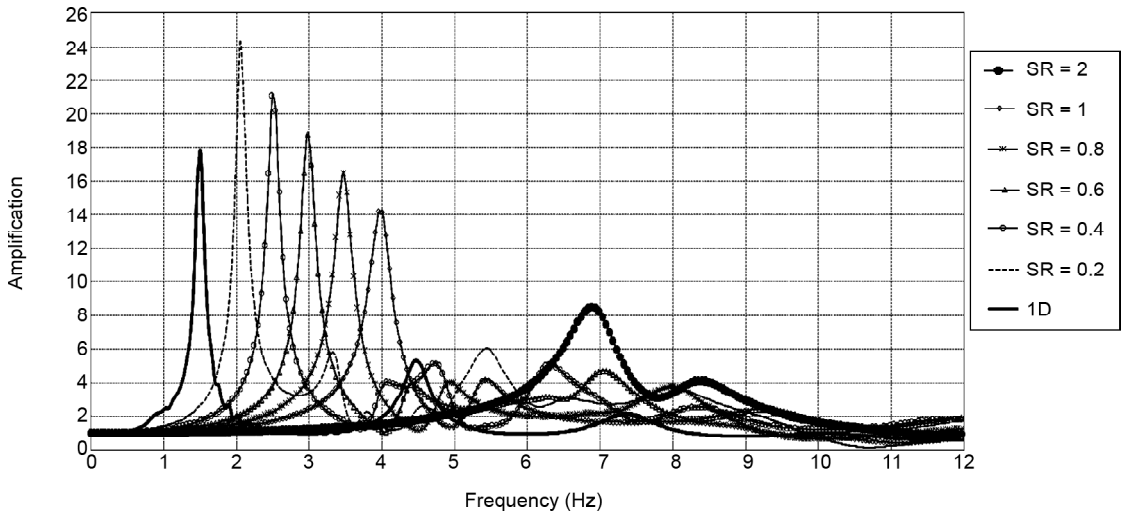

Figure 6. Amplification curves at top of the centerline of the triangular alluvial valley (Vs = 300 m/s) with different shape ratios.

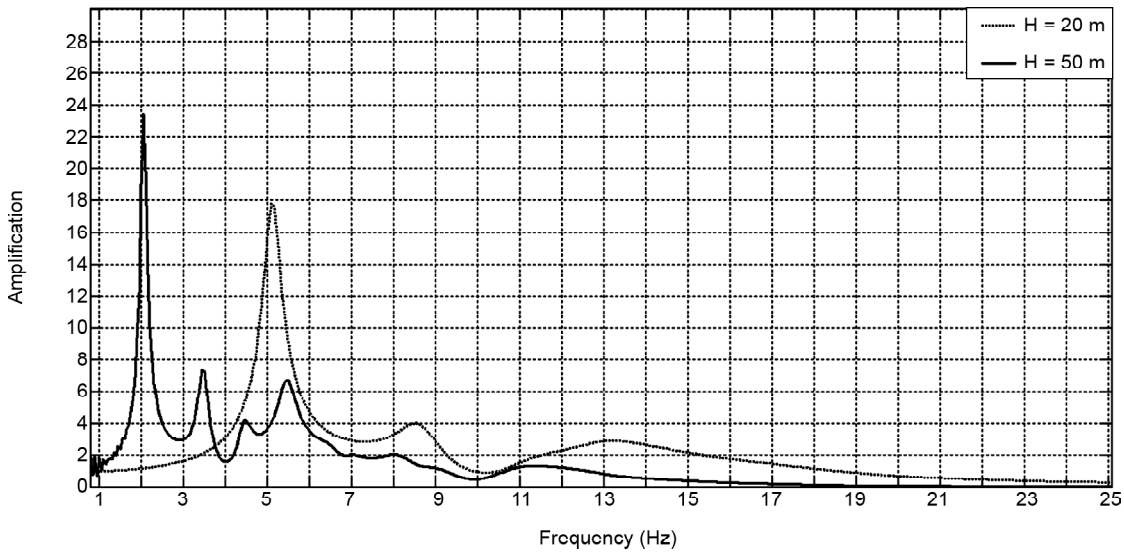

Figure 7. Amplification curves at top of the centerline of two different valleys possessing a constant shape ratio of 0.2 with a thickness of the soil layer at the center line of 50 and 20 meter (Vs = 300 m/s).

on the amplification curve of the center of 2D triangular alluvial valleys possessing a constant shape ratio of 0.2, subjected to vertically propagating incident SV waves. Two curves are presented that correspond to two different valleys with a thickness of the soil layer at the center line of 50 and 20 meter, respectively. The mechanical characteristics of the filling soil are the same in two valleys. As can be seen, the amplification pattern of the triangular alluvial valley and its frequency characteristics depend strongly on its dimension. When the shape ratio is kept constant, and the thickness of the valley increases, the natural frequency of the triangular alluvial valley decreases, and the amplification curve of the center node (2D case) moves towards the amplification curve of the corresponding 1D case. On the other hand, by increasing the thickness of the valley while shape ratio is kept constant, the maximum amplification of the ground surface increases. The main reason for this behavior is the ratio of the topography height to the wavelength of the propagated wave. In fact by increasing the thickness of the valley while the wavelength of the incident wave is constant, the repetition of a complete wave to travel from bedrock to surface increases, and it means that the incident wave amplifies more.

3.3. Natural Period of a Triangular Alluvial Valley

Extracting a simple formula in order to get an initial estimation of the natural period of a triangular alluvial valley could be useful in site effect microzonation studies. Figure (8) demonstrates how the natural frequency of the triangular alluvial valley alters with its shape ratio. Two curves are presented that correspond to two different alluviums with a shear wave velocity of 300 and 400 m/s, respectively. As can be seen, the curves are similar and infuse the idea of being capable to become non-dimensionalized. Figure (9) demonstrates these two curves once again, this time normalized to the natural frequency of the corresponding 1D uniform soil layer over the bed rock. As expected, the curves coincide and the ratio of the natural frequency of a triangular alluvial valley (F_{2D}) to the natural frequency of the corresponding 1D uniform soil layer over the bed rock (F_{1D}) can be approximated as a function of the shape ratio by the following formula:

$$F_{2D}/F_{1D} = 1.3 \cdot \exp(0.6 \cdot SR)$$

which can be re-written as:

$$F_{2D} = 1.3 \cdot \exp(0.6 \cdot SR) \cdot \left(V_s/(4 \cdot H)\right)$$

where, *Vs* represents shear wave velocity, *H* is triangular valley depth, and *SR* is the valley shape ratio (*SR*= *H/ax*).

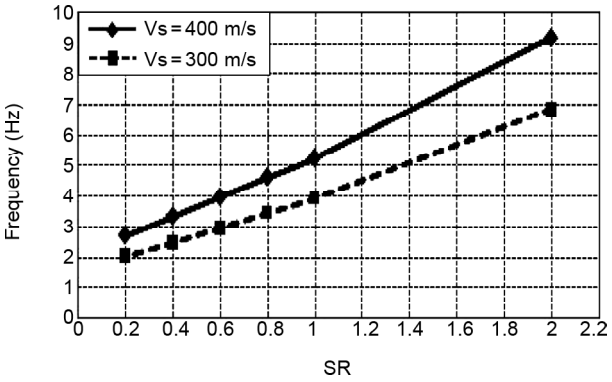

Figure 8. Natural frequency of the rectangular alluvial valley via its shape ratio for two different shear wave velocities of 300 and 400 m/s.

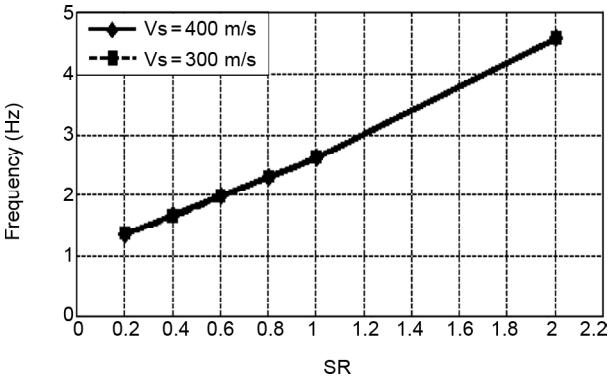

Figure 9. Dimensionless frequency of the triangular alluvial valley via its shape ratio.

4. Comparison of Seismic Response between Triangular and Rectangular Alluvial Valleys

At this point, it is of interest to compare the response spectra obtained for triangular alluvial valleys in this study with one derived for rectangular alluvial valleys, in order to identify the effects of topographical characteristics on seismic response of valleys. The amplification curves of various nodes along the ground surface of rectangular alluvial valley via the different shape ratios were presented in order to specify the effect of each parameter on

seismic response of rectangular alluvial valleys in previous works [45]. Figure (10) compares the amplification curves of the center of the triangular alluvial valley with those of the corresponding rectangular alluvial valley in each shape ratio. As can be seen, in a distinctive shape ratio always the value of natural frequency of the triangular alluvial valley is bigger than the natural frequency of the rectangular alluvial valley. One other important subject in Figure (10) is that the value of amplification of the center point of rectangular alluvial valley is bigger than the triangle alluvial valley except for shape ratio of 0.2.

Figure (11) illustrates the maximum amplification of various nodes along the ground surface of triangular alluvial valley normalized to the maximum amplification of a 1D uniform homogeneous soil layer resting on a rigid bed rock (amplification ratio) in comparison with those of the corresponding rectangular alluvial valley in each shape ratio. Once again, it is obvious that the greatest amount of amplification that occurs at the center point of the ground surface of each valley is bigger in rectangular alluvial valleys than in triangle alluvial valleys except for shape ratio of 0.2. A prominent point in Figure (11) is that in almost all shape ratios, the curve of the maximum amplification ratio of various nodes along the ground surface of triangular alluvial valley is completely under the curve of the rectangular valley. Only in shape ratio of 0.2 and 2 this rule is not true and the main reason for this behavior can be explained by considering the edge effects of

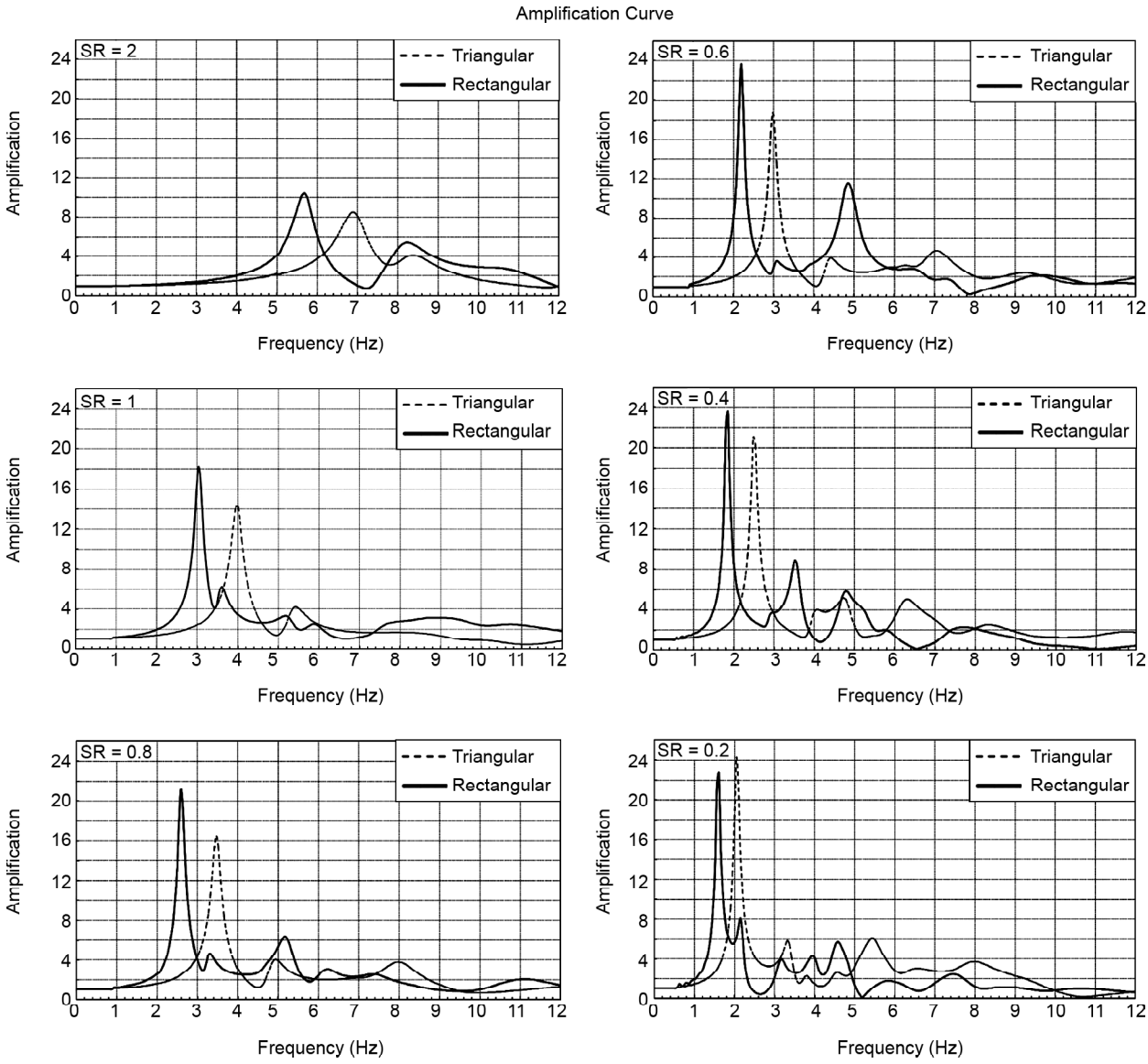

Figure 10. Comparison of the amplification curves of the center of the triangular and rectangular alluvial valleys via the different shape ratios.

valley in scattering the incident and reflected waves.

Figure (12) demonstrates how the natural frequency of the triangular and rectangular alluvial valleys normalized to the natural frequency of the corresponding 1D uniform soil layer alter with their

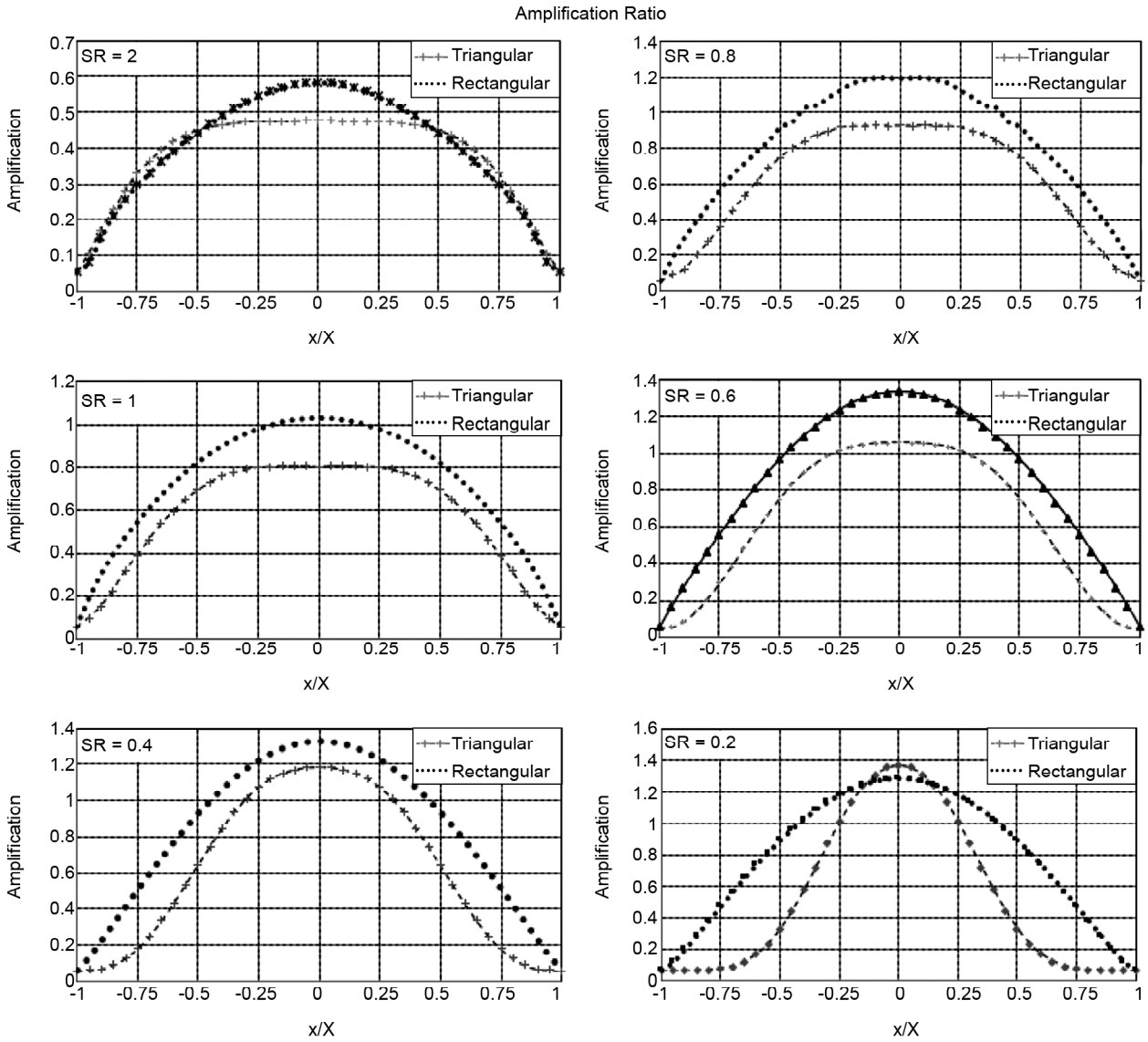

Figure 11. Maximum amplification of various nodes along the ground surface of triangular alluvial valley normalized to the maximum amplification of a 1D uniform homogeneous soil layer in comparison with those of the corresponding rectangular alluvial valley in each shape ratio.

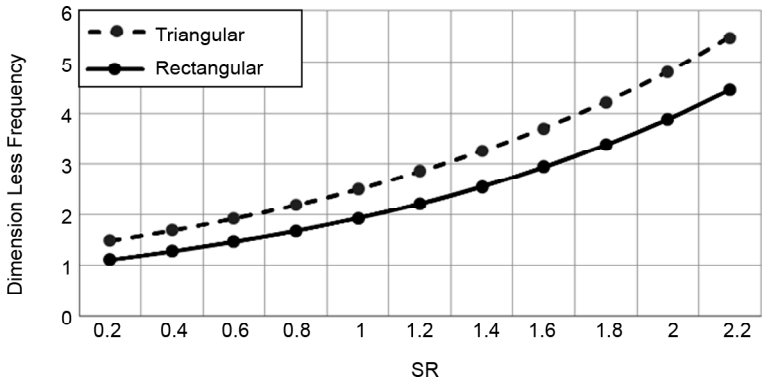

Figure 12. Dimensionless frequency of the triangular and rectangular alluvial valleys via the different shape ratios.

shape ratios. As can be seen, the dimensionless frequency of the triangular alluvial valley in each shape ratio is bigger than that of the rectangular alluvial valley. The volume of alluvium in a triangular valley is less than the amount of alluvium in the corresponding rectangular valley. That is why the behavior of the triangular alluvial valley is more similar to the behavior of a rock outcrop.

5. Conclusion

This paper is concerned with the problem of soil amplification and seismic site effects due to the local topographical and geotechnical characteristics. It has been conducted as an attempt to capture the significant 2D valley effects on the amplitude and the variability of ground shaking of the triangular and rectangular alluvial valleys. All calculations are executed in time-domain utilizing a linear spectral finite element method under SV excitation. It is shown that the amplification pattern of an alluvial valley and its frequency characteristics depend strongly on its shape ratio. A natural frequency can be defined for the triangular and rectangular alluvial valleys so that at all nodes along the ground surface, the highest amplification factor occurs at this predominant frequency. The natural frequency of the alluvial valley decreases towards the natural frequency of the corresponding 1D uniform soil layer on bed rock, as the shape ratio of the valley decreases. The maximum amplification ratio along the ground surface occurs at the center of the valley and decreases when one moves towards the corners. A simple formula has been proposed for initial estimation of the natural period of triangular alluvial valleys, which can be used in site effect microzonation studies. Comparison of seismic response between the triangular and rectangular alluvial valleys specifies that in a distinctive shape ratio always the value of natural frequency of the triangular alluvial valley is bigger than the natural frequency of the corresponding rectangular alluvial valley.

References

1. Aki, K. and Larner, K.L. (1970) Surface motion of a layered medium having an irregular interface due to incident plane SH waves. *Journal of Geophysical Research*, **75**, 933-954.
2. Aki, K. (1988) Local site effects on strong ground motion. *Earthquake Engineering and Soil Dynamics II*, ASCE.
3. Aki, K. (1993) Local site effects on weak and strong ground motion. *Tectonophysics*, **218**, 93-111.
4. Trifunac, M.D. (1971) Surface motion of a semi-cylindrical alluvial valley for incident plane SH waves. *Bulletin of the Seismological Society of America*, **61**, 1755-1770.
5. Sanchez-Sesma, F.J. and Esquivel, J.A. (1979) Ground motion on alluvial valleys under incident plane SH waves. *Bulletin of the Seismological Society of America*, **69**, 1107-1120.
6. Bard, P.Y. and Bouchon, M.A. (1980) The seismic response of sediment filled valleys, Parts I-II. *Bulletin of the Seismological Society of America*, **70**.
7. Sanchez-Sesma, F.J., Chavez-Garcia, F., and Bravo, M.A. (1988) Seismic response of a class of alluvial valley for incident SH waves. *Bulletin of the Seismological Society of America*, **78**(1), 83-95.
8. Graves, R.W. (1996) Simulating seismic wave propagation in 3-D elastic media using staggered grid finite differences. *Bulletin of the Seismological Society of America*, **86**, 1091-1106.
9. Bao, H., Bielak, J., Ghattas, O., Kallivokas, L.F., O'Hallaron, D.R., Shewchuk, J., and Xu, J. (1996) Earthquake ground motion modeling on parallel computers. *Proc. ACM W IEEE Supercomputing Conference*, Pittsburgh, USA.
10. Bard, P.Y. (1997) Local effects on strong ground motion: Basic physical phenomena and estimation methods for microzoning studies. *Notes of the Advanced Study Course SERINA (Seismic Risk: An Integrated Seismological*, Geotechnical and Structural Approach), Thessaloniki, Greece.
11. Faccioli, E., Maggio, F., Paolucci, R., and Quarteroni, A. (1997) 2-D and 3-D elastic wave propagation by a pseudo-spectral domain decomposition method. *Journal of Seismology*, **1**, 237-251.

12. Kokusho, T. and Matsumoto, M. (1998) Nonlinearity in site amplification and soil properties during the 1995 Hyogoken-Nambu earthquake. *Special Issue of Soils and Foundations*, **2**, 1-9.

13. Bielak, J., Xu, J. and Ghattas, O. (1999) Earthquake ground motion and structural response in alluvial valleys. *Journal of Geotechnical and Geoenvironmental Engineering*, **125**, 413-423.

14. Paolucci, R. (1999) Fundamental vibration frequencies of 2-D geological structures. *Proc. 2nd International Conference on Earthquake Geotechnical Engineering*, Lisbon, **1**, 255-260.

15. Finn, W.D.L. (1991) Geotechnical engineering aspects of seismic microzonation. *Proc. 4th International Conference on Seismic Zonation*, Stanford, **1**, 199-250.

16. Yegian, M.K., Ghahraman, V.G., and Gazetas, G. (1994) Seismological, soil and valley effects in Kirovakan, 1988 Armenia earthquake. *Journal of Geotechnical Engineering*, ASCE, **120**(2), 349-365.

17. Bardet, J.P., Kapuskar, M., Martin, G.R., and Proubet, J. (1992) *Site Response of the Marina District of San Francisco during the Loma Prieta Earthquake*. USGS Professional Paper 1551-F, the Loma Prieta, California, Earthquake of October 17, 1989- Marina District, 85-140.

18. Graves, R.W. (1993) Modeling three-dimensional site response effects in the marina district basin, San Francisco, California. *Bulletin of the Seismological Society of America*, **83**, 1042-1063.

19. Zhang, B. and Papageorgiou, A.S. (1996) Simulation of the response of the Marina district basin, San Francisco, CA., to the 1989 Loma Prieta Earthquake. *Bulletin of the Seismological Society of America*, **86**(5), 1382-140.

20. Graves, R.W. (1998) Three-dimensional computer simulations of realistic earthquake ground motions in regions of deep sedimentary basins. *2nd International Symposium on the Effects of Surface Geo-Seismic Motion*, Yokohama, I, 103-120.

21. Kawase, H. (1996) The cause of the damage belt in Kobe: "The basin-edge effect", Constructive interference of the direct S-wave with the basin-induced diffracted Rayleigh waves. *Seismological Research Letters*, **67**(5), 25-34.

22. Takemiya, H. (1996) Effects of irregular soil profile on strong ground motion, The 1995 Hyogoken-Nanbu Earthquake. *Japan Society of Civil Engineers*, 15-26.

23. Pitarka, A., Irikura, K., Iwata, T., and Sekiguchi H. (1998) Three-dimensional simulation of the near-fault ground motion for the 1995 Hyogoken-Nambu, Japan, earthquake. *Bulletin of the Seismological Society of America*, **88**, 428-440.

24. Matsushima, S. and Kawase, H. (1998) 3-D wave propagation analysis in Kobe referring to "The basin-edge effect". *2nd International Symposium on the Effects of Surface Geology on Seismic Motion*, Yokohama, III, 1377-1384.

25. Hisada, Y., Bao, H., Bielak, J., Ghattas, O., and O'Hallaron, D.R. (1998) Simulations of long-period ground motions during the 1995 Hyogoken-Nambu (Kobe) earthquake using 3-D finite element method. *2nd International Symposium on the Effects of Surface Geology on Seismic Motion*, Yokohama, III, 1353-1360.

26. Trifunac, M.D. and Hudson, D.E. (1971) Analysis of the Pacoima Dam accelerograms: San Fernando earthquake of 1971. *Bull. Seism. Soc. Am.*, **61**, 1393-1411.

27. Wong, H.L. and Trifunac, M.D. (1974) Surface motion of semielliptical alluvial valley for incident plane SH wave. *Bull. Seismological Soc. of Am.*, 64, 1389-1408.

28. Sa´nchez-Sesma, F.J. (1983) Diffraction of elastic waves by three-dimensional surface irregularities. *Bull. Seismological Soc. of Am.*, **73**, 1621-1636.

29. Lee, V.W. (1990) Scattering of plane SH waves by a semi-parabolic cylindrical canyon in an elastic half-space. *Int. J. Geophys.*, **100**, 79-86.

30. Alterman, Z.S. and Karal, F.C. (1968) Propagation of elastic waves in layered media by finite difference methods. *Bull. Seismological Soc. of*

Am., **58**, 367-398.

31. Boore, D.M. (1972) Finite difference methods for seismic wave propagation in heterogeneous materials. Methods in computational physics. *B.A. Bolt, ed.*, **11**, Academic Press, New York.

32. Frankel, A. (1993) Three-dimensional simulations of ground motions in the San Bernardino Valley, California, for hypothetical earthquakes on the San Andreas Fault. *Bull. Seismological Soc. of Am.*, **83**, 1020-1041.

33. Lysmer, J. and Drake, L.A. (1971) The propagation of Love waves across nonhorizontally layered structures. *Bull. Seismological Soc. of Am.*, **61**, 1233-1252.

34. Smith, W.D. (1975) The application of finite lement analysis to body wave propagation problems. *J. Geophys.*, **44**, 747-768.

35. Li, X., Bielak, J., and Ghattas, O. (1992) Three-dimensional earthquake response on a CM-2. *Proc., 10th World Conf. Earthquake Engrg.*, 2, Balkema, Rotterdam, The Netherlands, 959-964.

36. Toshinawa, T. and Ohmachi, T. (1992) Love wave propagation in a three-dimensional sedimentary basin. *Bull. Seismological Soc. of Am.*, **82**, 1661-1667.

37. Bouchon, M. and Aki, K. (1977) Discrete wavenumber representation of seismic source wavefield. *Bull. Seismological Soc. of Am.*, **67**, 259-277.

38. Bard, P.Y. and Bouchon, M. (1985) The two-dimensional resonance of sediment-filled valleys. *Bull. Seismological Soc. of Am.*, **75**, 519-541.

39. Kawase H. (1988) Time-domain response of a semicircular canyon for incident SV, P and Rayleigh waves calculated by the discrete wavenumber boundary element method. *Bull. Seismol. Soc. Am.*, **78**, 1415-37.

40. Sa´nchez-Sesma, F.J., Ramos-Mart´nez, J., and Campillo, M. (1993) An indirect boundary element method applied to simulate the seismic respond of alluvial valleys for incident P, S and Rayleigh waves. *Earthquake Engrg. and Struct. Dyn.*, **22**, 279-295.

41. Kamalian, M., Gatmiri, B., Sohrabi-Bidar, A., and Khalaj, A. (2007) Amplification pattern of 2D semi-sine-shaped valleys subjected to vertically propagating incident waves. *Communications in Numerical Methods in Engineering*, **23**, 871-887.

42. Sohrabi-bidar, A., Kamalian, M., and Jafari, M.K. (2009) Time-domain BEM for three-dimensional site response analysis of topographic structures. Int. *Journal Numer. Meth. Engng.*, **79**, 1467-1492.

43. Sohrabi-bidar, A., Kamalian, M., and Jafari, M.K. (2010) Seismic response of 3-D Gaussian--shaped valleys to vertically propagating incident waves. *Geophys. J. Int.*, **183**, 1429-1442

44. Mossessian, T. and Dravinski, M. (1987) Application of a hybrid method for scattering of P, SV, and Rayleigh waves by near-surface irregularities. *Bull. Seismological Soc. of Am.*, **77**, 1784-1803.

45. Najafizadeh, J., Kamalian. M, Jafari, M.K., and Khaji, N. (2014) Seismic Analysis of Rectangular Alluvial Valleys Subjected to Incident Sv Waves by Using the Spectral Finite Element Method. *International Journal of Civil Engineering* (Ijce) (Accepted).

46. Psarropoulos, P.N., Tazoh, T., Gazetas, G., and Apostolouiv, M. (2007) Linear and nonlinear valley amplification effects on seismic ground motion. *Soils and Foundations, Japanese Geotechnical Society*, **47**(5), 857-871.

47. Komatitsch, D. and Tromp, J. (1999) Introduction to the spectral element method for three-dimensional seismic wave propagation. *Geophys. J. Int.*, **139**, 806-822.

48. Kamalian, M., Jafari, M.K., Sohrabi Bidar, A., and Razmkhah, A. (2008) Seismic response of 2D semi-sine shaped hills to vertically propagating incident waves: amplification patterns and engineering applications. Earthquake Spectra, **24**(2), 405-430.